nature biotechnology

LETTERS

https://doi.org/10.1038/s41587-020-0468-5

Check for updates

Genetic circuit design automation for the gut resident species *Bacteroides thetaiotaomicron*

Mao Taketani[1,2], Jianbo Zhang[1], Shuyi Zhang[1], Alexander J. Triassi[1], Yu-Ja Huang[1], Linda G. Griffith[1] and Christopher A. Voigt[1]✉

***Bacteroides thetaiotaomicron* is a human-associated bacterium that holds promise for delivery of therapies in the gut microbiome[1]. Therapeutic bacteria would benefit from the ability to turn on different programs of gene expression in response to conditions inside and outside of the gut; however, the availability of regulatory parts, and methods to combine them, have been limited in *B. thetaiotaomicron*[2–5]. We report implementation of Cello circuit design automation software[6] for this species. First, we characterize a set of genome-integrated NOT/NOR gates based on single guide RNAs (CRISPR-dCas9) to inform a *Bt* user constraint file (UCF) for Cello. Then, logic circuits are designed to integrate sensors that respond to bile acid and anhydrotetracycline (aTc), including one created to distinguish between environments associated with bioproduction, the human gut, and after release. This circuit was found to be stable under laboratory conditions for at least 12 days and to function in bacteria associated with a primary colonic epithelial monolayer in an in vitro human gut model system.**

Engineered bacteria can function as 'smart' therapeutics to deliver a drug or vaccine, to detect or prevent infections, and to respond to physiological changes[7]. Although it is possible to express a therapeutic payload continuously, it would be useful if bacteria could be engineered to respond to environmental signals; for example, to trigger drug release in a particular microenvironment, to maintain a treatment at specific levels, or to switch a therapy on or off in the body[8–11]. *Bacteroides* are Gram-negative obligate anaerobes that compose a third of the bacteria found in fecal material[12–19]. They are attractive candidate vectors for therapies owing to their stable colonization of the mammalian colon and modulation of the host immune system. They have been studied as treatments of colitis and autism, and strains have been engineered to improve engraftment and bio-containment[20–22]. Tools for genetic manipulation have been reported[2–4,23], but predictively combining these parts to create more complex functions, including genetic circuits, remains a challenge.

Bacteria residing in the body can be engineered to respond to in situ conditions, small molecules present in food or water, and to distinguish disease states, including inflammation, fever, intestinal bleeding, tumors and pathogens[2,3,20,24–34]. Small molecule sensors have been developed for *Bacteroides* species to induce expression when colonized in a host[2,3,20]. As an endogenous signal, bile acids offer a means to identify regions within the gut. Gradients of bile acid variants are formed as they are released into the duodenum and are chemically modified by bacteria as they transit the length of the intestines[35–40]. The human large intestine has ~500 mM bile acids, one-third of which is deoxycholic acid (DCA)[41]. Changes in bile acid composition have been shown to correlate with the onset of colon or liver cancer, genetic disorders, obesity, diabetes, and inflammation[36,42–44]. Some pathogenic bacteria use TetR homologues to respond to bile acids[45–47]. Based on a bacterial regulator, a synthetic bile acid sensor has been constructed in mammalian cells[48].

Sensors alone can only produce a simple response. Genetic circuits can implement more complex signal processing; for example, logic to identify an environment, periodic drug delivery, diagnostic memory, or communicating to control toxin release[4,26,32,49,50]. Cello (www.cellocad.org) was developed to automate circuit design and make it easier to incorporate synthetic regulation into genetic engineering projects[6]. The inputs to Cello are the sensors, the desired circuit function (in Verilog), and a user constraint file (UCF) that specifies organism, genetic location, gate technology and mapping constraints[51]. The first UCF (Eco1C1G1T1) is specific to *Escherichia coli* NEB10β for circuits on a p15a plasmid and contains 12 repressor-based NOR/NOT gates. Cello uses the response function of the gates (how the output promoter changes as a function of the input promoter) to connect them to create the specified circuit. Connecting gates to each other and to sensors requires that their inputs and outputs share a common signal carrier, defined to be the RNA polymerase (RNAP) flux and measured in relative promoter units (RPUs) as a ratio to a reference promoter[52]. Designed circuits function as specified in *E. coli*; however, it is not possible to simply use Eco1C1G1T1 for other bacterial species.

The first step in implementing circuit design automation for a new host is to define a reference promoter to use when characterizing sensor and gate promoters in RPUs. *E. coli* promoters do not work well in *Bacteroides*, so we selected a different constitutive promoter for this purpose (P_{PAM3}) and a reference strain was constructed (*B. thetaiotaomicron* strain MT768) (Fig. 1a and Supplementary Fig. 1)[2]. As green fluorescent protein (GFP) requires oxygen for chromophore maturation and is only visible in *Bacteroides* when highly expressed[4], we opted to use luciferase (*nanoluc*) as our reporter gene[53]. Luminescence from P_{PAM3} is measured and normalized by cell density (Methods). The resulting value is defined as $RPU_L = 1$ and used to normalize the activity of other promoters (Fig. 1b).

Next, we constructed a bile acid sensor. First, we compiled a list of known and putative repressors that respond to bile acids, including CmeR (*C. jejuni*) and BreR (*Vibrio cholerae*) and six putative regulators (VFA0359, BCAS0007, Bamb6005, VFA0088, Smlt2112 and Xcc0233)[45,47,48,54,55]. A sensor was constructed based on each repressor by placing the gene under the control of a constitutive promoter (Fig. 1c). An output promoter was designed by placing the operator sequence between the −33 and −7 region of a constitutive promoter

[1]Department of Biological Engineering, Massachusetts Institute of Technology, Cambridge, MA, USA. [2]Present address: DeepBiome Therapeutics, Cambridge, MA, USA. ✉e-mail: cavoigt@gmail.com

(P_{cfxA}). The sensors were integrated into attBT1-1. Cells were grown in the presence and absence of 62.5 µM DCA for 6 h in TYG (tryptone–yeast extract–glucose) media under anaerobic conditions and then the promoter activity was measured (Supplementary Fig. 2 and Methods). The sensor based on VFA0359 produced a superior response, with a low basal activity, 440-fold dynamic range, and half-maximum at 8 µM DCA (Fig. 1d and Supplementary Fig. 3). This sensor was evaluated for its response to other bile acids and it was found that DCA > LCA > CDCA > CA (Supplementary Fig. 4 and Supplementary Table 1). No response for conjugated bile acids (TCA and GCA) was observed (not shown).

We tested the VFA0359 bile acid sensor for cross-talk with the aTc and IPTG (isopropyl-β-D-thiogalactoside) sensors developed previously for *B. thetaiotaomicron*[2,3]. Each sensor was divided such that the repressors and the output promoter and reporter were integrated into different locations in the *B. thetaiotaomicron* genome. All three repressors were transcribed from the P_{BT1311} constitutive promoter and the cassette was inserted into attBT-1. The output promoters (P_{BA}, P_{LacO23} and $P1T_{DP}$) drive *nanoluc* expression and are integrated at one (DCA) or two (IPTG and aTc) sites in the genome. The sensors were evaluated for their response to DCA, IPTG and aTc, and no cross-talk was observed (Fig. 1e and Supplementary Figs. 5–7). There is also no cross-talk between repressors and promoters (Supplementary Figs. 5–7).

Genetic circuits can be constructed by combining gates that perform simpler logic operations. We chose to base the gate technology

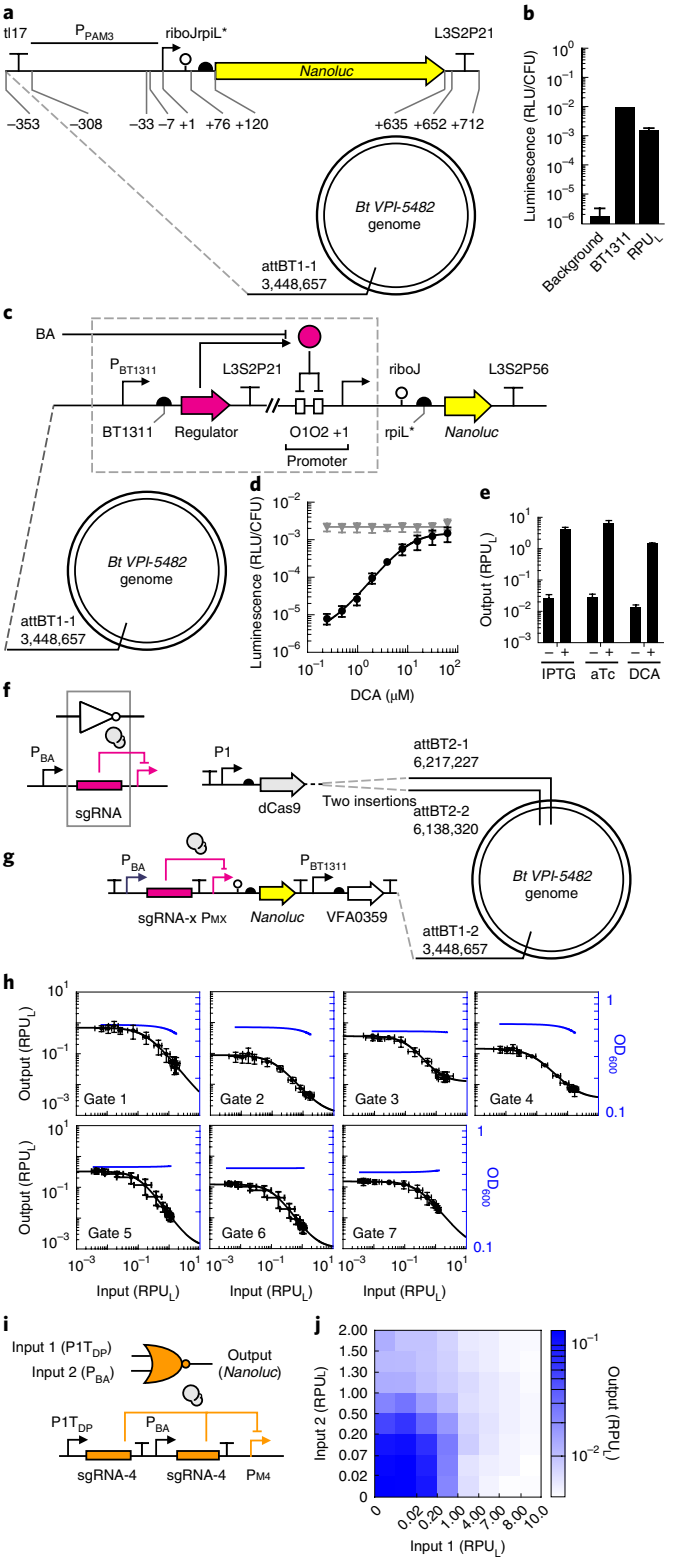

Fig. 1 | Sensor, NOT and NOR gate characterization in *B. thetaiotaomicron*. **a**, Schematic of the promoter standard (P_{PAM3}) used to measure RPU_L (*B. thetaiotaomicron* MT768). **b**, The luminescence activity of the strong promoter P_{BT1311} (sourced from ref. [28]) and the background luminescence from *B. thetaiotaomicron* (*Bt*) (strain MT767) is compared to the RPU_L standard (Methods). **c**, The design of the bile acid sensors and its location in the genome (*B. thetaiotaomicron* MT329). The 'regulator' gene represents the bile acid binding proteins tested and the corresponding operator is placed in two locations in the promoter. **d**, The response of the bile acid sensor to DCA (Methods). The gray line is the response of the parent promoter P_{cfxA}. **e**, The responses of the sensors to no inducer and the presence of inducer (500 µM IPTG, 100 ng µL^{-1} aTc, and 62.5 µM DCA) (*B. thetaiotaomicron* MT770, MT771 and MT772) (Methods). These values are used as the inputs to Cello for circuit design. For **a**, **b** and **c**, the sequences of genetic parts are provided in Supplementary Table 5. The data represent the average of three replicates collected on different days and error bars correspond to the standard deviation between these measurements. **f**, The inverter function is performed by dCas9 (gray circles) directed to a promoter by a sgRNA. The output promoter of the bile acid sensor (P_{BA}) is used to characterize gate function. **g**, The characterization system for measuring the response functions of NOT gates. dCas9 is constitutively expressed from the P1 promoter. The bile acid sensor is used to turn on the NOT gate (P_{BA}). Note that the strains also contain the aTc and IPTG sensors, which are removed here for clarity (see Supplementary Fig. 13). Each NOT gate (*x* from 1 to 7) required the construction of a different strain for characterization: *B. thetaiotaomicron* MT773–MT775, MT782, MT804–MT806. The sequences of the NOT gates, including all component parts, are provided in Supplementary Table 6. **h**, The response function for each NOT gate (Methods). The input to the gate is the bile acid sensor induced by DCA (left to right, 0, 0.4, 0.6, 1.0, 1.7, 2.9, 4.9, 8.1, 13.5, 22.5, 37.5 and 62.5 µM). The input (*x* axis) is converted to RPU_L by separately measuring the activity of P_{BA} for these concentrations (Supplementary Fig. 14). The black lines are fits to the Hill function (parameters in Supplementary Table 2). The blue lines show the impact of gate induction on cell growth (a regression curve is shown, fit to the OD_{600} data in Supplementary Fig. 15). The data represent the average of three replicates collected on different days, and error bars correspond to the standard deviation between these measurements. **i**, The 'split' design of the NOR gate, where each input promoter drives a separate copy of the same gRNA. **j**, The luminescence of the NOR gate is shown as a function of the activity of the two input promoters. The bile acid sensor was converted from µM DCA to RPU_L as described in part **h** (bottom to top, 0, 0.9, 1.9, 3.9, 7.8, 15.6, 31.25 and 62.5 µM DCA). The second input was induced by aTc and converted to RPU_L similarly (left to right, 0, 0.4, 1.0, 2.6, 6.4, 16, 40, 100 ng µl^{-1} of aTc) (Supplementary Fig. 19). The data represent the average of three replicates collected on different days.

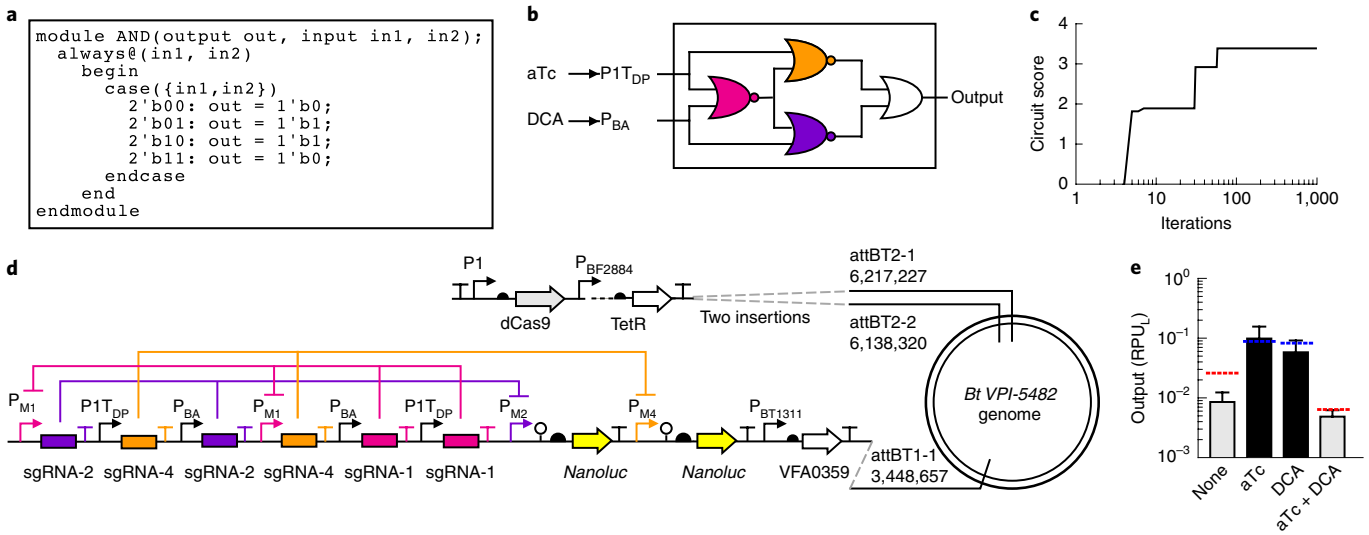

Fig. 2 | Automated design of an XOR circuit. a, The XOR gate is specified using the Verilog description language. **b**, Cello identifies the wiring diagram of NOR/OR gates that produces the XOR function. The two sensors are defined (aTc and DCA) as well as their off and on states in RPU_L (Fig. 1e). Each gate is then assigned a sgRNA (colors). **c**, The simulated annealing run for gate assignment. Circuit score is defined by the lowest output state that should be on divided by the highest output state that should be off. Different sgRNAs are permuted between gates until it converges on the solution shown in part b. **d**, The genome organization of the circuit, as specified by Cello. Note that the IPTG sensor is also present at the attBT2-1 and attBT2-2 sites (dots, see Supplementary Fig. 20). **e**, The colored lines show the predicted response to different combinations of inputs (the presence and absence of 100 ng μl^{-1} aTc and 62.5 µM DCA). The dashed lines are colored blue for the on states and red for the off states. The predictions are made by Cello by mathematically combining the gate response functions. The experimental measurements are shown as gray and black bars for the off and on states, respectively (Methods). The data represent the average of three replicates collected on different days and error bars correspond to the standard deviation between these measurements.

on the two-input NOR function, which has two input promoters and one output promoter. Previously, we used protein repressors to implement the inversion function[56], but we found that these do not produce sufficient dynamic range when moved to the *B. thetaiotaomicron* genome (not shown). As an alternative, we implement this function with CRISPR interference using a small guide RNA (sgRNA) to direct deactivated Cas9 (dCas9) to repress a target promoter (Fig. 1f). This approach has been used previously by ourselves and others to build genetic logic in *E. coli* and *S. cerevisiae*[2,57–60]. Although toxicity has been observed when dCas9 is expressed in *E. coli*[58], no growth impact is observed in *B. thetaiotaomicron* (Supplementary Fig. 8).

Each gate is based on a different sgRNA. The sgRNAs were designed by randomizing the DNA recognition sequence and computationally scanning the genome to ensure its absence (Methods). Repressible promoters were designed by placing the corresponding target sequence in different positions in P_{BF2884} and screening for the highest repression, which occurs just upstream of the −7 position (P_{Msite3}) (Supplementary Fig. 9). When 62.5 µM DCA is added to induce sgRNA transcription, this leads to a 20-fold reduction in luminescence (Methods). Additional sgRNAs were designed to create an orthogonal set of seven gates (Supplementary Figs. 10,11) (Methods). Although a much larger library is possible, we found in *E. coli* that additional sgRNAs above 7 cannot be used in a single circuit without significantly drawing down the dCas9 resource and reducing the gate response to <10-fold[58,61].

Gates require strong terminators to avoid read-through to other gates or chromosomal genes. In addition, each gate should use a different terminator to avoid repeated DNA sequences that might cause recombination while constructing or carrying the circuit. Terminators have not been well-characterized in *Bacteroides*, so we chose several strong terminators from an *E. coli* library[62] and designed a system to quantify their strength in *B. thetaiotaomicron* (Methods and Supplementary Fig. 12).

NOT gates were constructed based on the sgRNAs, promoters and terminators. The expression of dCas9 is controlled by the constitutive P1 promoter (Fig. 1g and Supplementary Fig. 13). The response function of each gate was measured by increasing the concentration of DCA and measuring the response of the gate output promoter in RPU_L (Fig. 1h and Supplementary Figs 14,15) (Methods). However, to predict how to connect gates, the input also has to be reported in RPU_L, not DCA concentration. To correct the response functions, a separate strain (*B. thetaiotaomicron* strain MT772) was constructed to measure the activity of the P_{BA} promoter as a function of DCA and these data are used to correct the *x* axes of the response functions (Supplementary Fig. 14). The corrected response functions were fit to a mathematical form, from which the parameters were extracted (Supplementary Table 2).

The NOT gates can be converted to NOR gates by adding a second input promoter. To avoid the roadblocking that can occur with tandem promoters[23], we opted to construct NOR gates by creating a duplicate copy of the sgRNA (and its associated terminator) and placing each under the control of a different input promoter (Fig. 1i and Supplementary Figs. 16,17). NOR gates are characterized by a two-dimensional response function (Fig. 1j), but the design automation algorithm is simplified if it can be based on their one-dimensional NOT response functions (Fig. 1h) and using the sum of the input promoter activities. Experiments were designed to test whether this is sufficiently accurate and, indeed, the NOT gate response functions can be used (Supplementary Fig. 16).

The DNA sequence, parameterization of the response function, and growth impact (measured as optical density at 600 nm (OD_{600})) of each gate were combined to build a UCF for *B. thetaiotaomicron* (Bth1C1G1T1, Supplementary File 1). The specified organism is *B. thetaiotaomicron VPI-5482* with a cassette in attBT2-1 and attBT2-2 for the constitutive expression of dCas9. Eugene rules are included in the UCF to specify that the gates appear in the forward direction upstream of the output (Supplementary Fig. 18). A final

OR gate is implemented by splitting the last promoter to drive two copies of the output gene (for example, *nanoluc*). The UCF specifies that the circuit should be inserted into attBT1-1.

Cello was used to design logic circuits that can integrate the bile acid and aTc sensors. The logic operation can be specified in Verilog, either as a desired truth table or a specific wiring diagram. Once run, algorithms optimize the assignment of sgRNAs to each gate and then assemble the sequences to form the linear DNA encoding the circuit. Predictions are made for the expression of the output gene in response to all combinations of inputs (the presence and absence of aTc and DCA). Because the response functions are based on luciferase measurements, they represent cell population averages.

First, we designed a circuit that implements XOR logic: the output is on when either, but not both, inputs are on. Based on the truth table, written in Verilog (Fig. 2a), a logic minimization algorithm identifies the optimal wiring diagram (Fig. 2b). Then, the response functions of the sgRNA gates are used to calculate the optimal sgRNA for each position of the wiring diagram. This search is performed using a simulated annealing algorithm that seeks to maximize the difference between the highest output that should be off and the lowest output that should be on (circuit score) (Fig. 2c). Then, the Eugene rules are used to convert the assignment to a linear DNA sequence (Fig. 2d). The predicted responses are shown as the colored dashed lines in Fig. 2e. Note that these predictions were made prior to the construction of the circuit. The *B. thetaiotaomicron* strain containing the circuit was constructed exactly as specified. The response to the different combinations of inducers was measured and found to match closely to the predicted values (Fig. 2e).

Therapeutic bacteria would benefit from the ability to turn on different programs of gene expression at different stages. This can be achieved by multi-input multi-output logic that integrates a set of sensors to identify the environment. As a proof of principle, we envisioned a circuit designed to respond to signals corresponding to the conditions of a fermenter (inducer, but no bile acid), the gut environment (bile acid, but no inducer), and when expelled into the environment post treatment (no inducer and no bile acid) (Fig. 3a). Each of these is assigned a different output promoter that could then be used to control desired genes in each of these conditions. The desired logic was written in Verilog (Fig. 3b) and Cello designed the corresponding circuit and DNA sequence (Fig. 3c,d). To measure the outputs using the same reporter, three strains were constructed connecting each output promoter to *nanoluc*. Note that all three strains have the same circuit and all three output promoters, but null DNA sequences replace *nanoluc* for those not being measured (Fig. 3e). The output of the circuit closely matches the predictions across all 12 states representing the 4 combinations of inputs and 3 outputs (Fig. 3f).

To assess the long-term genetic stability of our circuits, strains were grown for 12 d and switched between states in a random progression in an anaerobic chamber. Cells were not carefully maintained in exponential phase during this growth experiment, with times when they were left in the anaerobic chamber for extended periods. This was done to stress the cells and to passage them through different growth conditions and nutrient levels. The circuits performed as predicted during this period, with no signs of breakage (Fig. 3g). The characteristic times for the circuit to go from off to on and from on to off are around 6 h.

A human gastrointestinal model[63] was used to test circuit function in the context of *B. thetaiotaomicron* cells adhered to a human epithelial monolayer. The monolayer covering the intestinal surface is faithfully recapitulated using primary colonic stem cell organoids that differentiate into absorptive, goblet and enteroendocrine cells (Fig. 4a) (Methods)[63]. Unlike models derived from cancer cell lines, the mucosal layer is secreted from goblet cells and more accurately reflects the coating of the human epithelium to which *B. thetaiotaomicron* naturally adheres (Fig. 4b)[64]. Upon adhering, *B. thetaiotaomicron* undergoes global changes in its transcriptome, seeks alternative carbon sources, and slows in growth[64]. Molecules secreted by cells in the epithelial layer, such as antimicrobial peptides, also impact the *B. thetaiotaomicron* transcriptome[65]. Using the gastrointestinal model allows us to prototype the performance of circuits in a realistic model of this cellular and environmental context.

Circuit performance was evaluated using the gastrointestinal model for the two-input three-output logic circuit. The epithelial monolayer is lined on a transwell insert with growth-supporting media for mammalian cells on the basolateral side (Fig 4a). Intrinsic to the evaluation of a circuit is the need to test the response to many combinations of inducers. To this end, the transwell system is ideal because the same epithelial monolayer can be established in a 12-well plate and the circuit response can be tested under identical conditions. Stem cells are seeded on a collagen-coated membrane of a transwell and differentiated for approximately 1 week (Fig. 4a,b). Separately, an overnight culture of *B. thetaiotaomicron* is resuspended in fresh pre-reduced yeast casitone fatty acid (YCFA) medium, of which 500 µl is introduced into the apical side of the monolayer and cultured for 2 h (Methods). DAPI (4,6-diamidino-2-phenylindole) and immunostaining of actin filaments indicate that *B. thetaiotaomicron* cells are localized to the apical side (Fig. 4c,d and Supplementary Figs. 21,22). The monolayer was verified to be intact as shown by brightfield images with no observable holes and transepithelial electrical resistance (TEER) values in the 'tight' GI epithelia range (Supplementary Fig. 23)[66].

After the bacteria adhere, the genetic circuit is induced by adding fresh media containing the appropriate combinations of DCA and aTc. The cells are cultured with the inducers for 6 h and the non-adhered cells are removed by pipetting. *B. thetaiotaomicron*

Fig. 3 | A circuit designed to integrate two sensors and control three programs of gene expression. a, The envisioned circuit, designed to respond to signals corresponding to the conditions of a fermenter, the gut environment, and when expelled into the environment post treatment. An output promoter for each combination of inputs allows different genes to be expressed under these conditions. The thick lines in the circuit indicate when the input promoters (aTc, $P1T_{DP}$; DCA, P_{BA}) or outputs are on. **b**, The Verilog specification of the truth table corresponding to the desired logic. **c**, Logic minimization algorithms identified the circuit diagram to produce the desired truth table using NOR gates. **d**, The simulated annealing run in Cello assigned sgRNAs to each gate. The best sets found are shown in **c**. **e**, The circuit was constructed as specified and inserted into the genome at the same position as shown in Fig. 2d. The same sensors and dCas9 cassette are inserted into the attBT2-1 and attBT2-2 sites (Supplementary Fig. 20). Three strains were constructed to report on the three output promoter activities (Output 1, *Bt* MT800; Output 2, *Bt* MT798; Output 3, *Bt* MT799). The black box indicates that the sequence was replaced with a null ATGTAA for promoters that are not being measured. **f**, Outputs of the two-input three-output circuits are shown. The predicted values for the three outputs are shown as blue (high) or red (low) lines. The inputs are the presence or absence of 100 ng μl^{-1} aTc and 62.5 µM DCA. The bars show the experimentally measured outputs expected to be low (gray) or high (black). The data represent the average of three replicates collected on different days and error bars correspond to the standard deviation between these measurements. **g**, A timecourse is shown in which the circuit is switched between states over more than 2 weeks (Methods). Each of the outputs was measured using the three reporter strains. The gray lines indicate when the transitions between inducer combinations occurred and the concentrations used are the same as above. The blue and red dashed lines are the values predicted by Cello for each combination of inputs.

cells located at the bottom of the apical chamber closely associated with the monolayer were collected by removing the top 450 µl of the culture and mixing the remaining 50 µl with 450 µl of fresh media. Their OD and luminescence were measured in the same manner as those samples in TYG culture. As seen in Fig. 4e, the output of the circuit closely matched that of the in vitro results

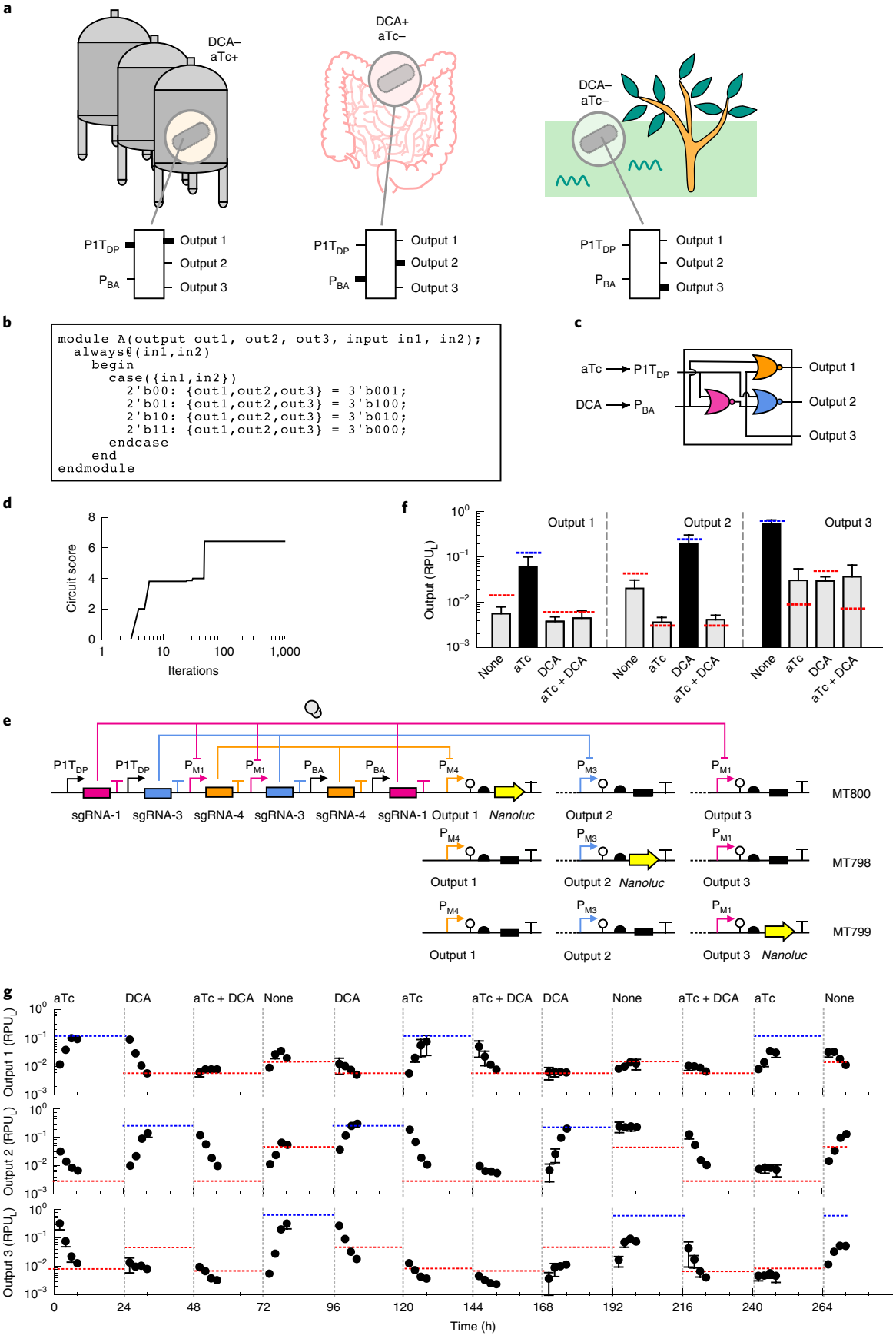

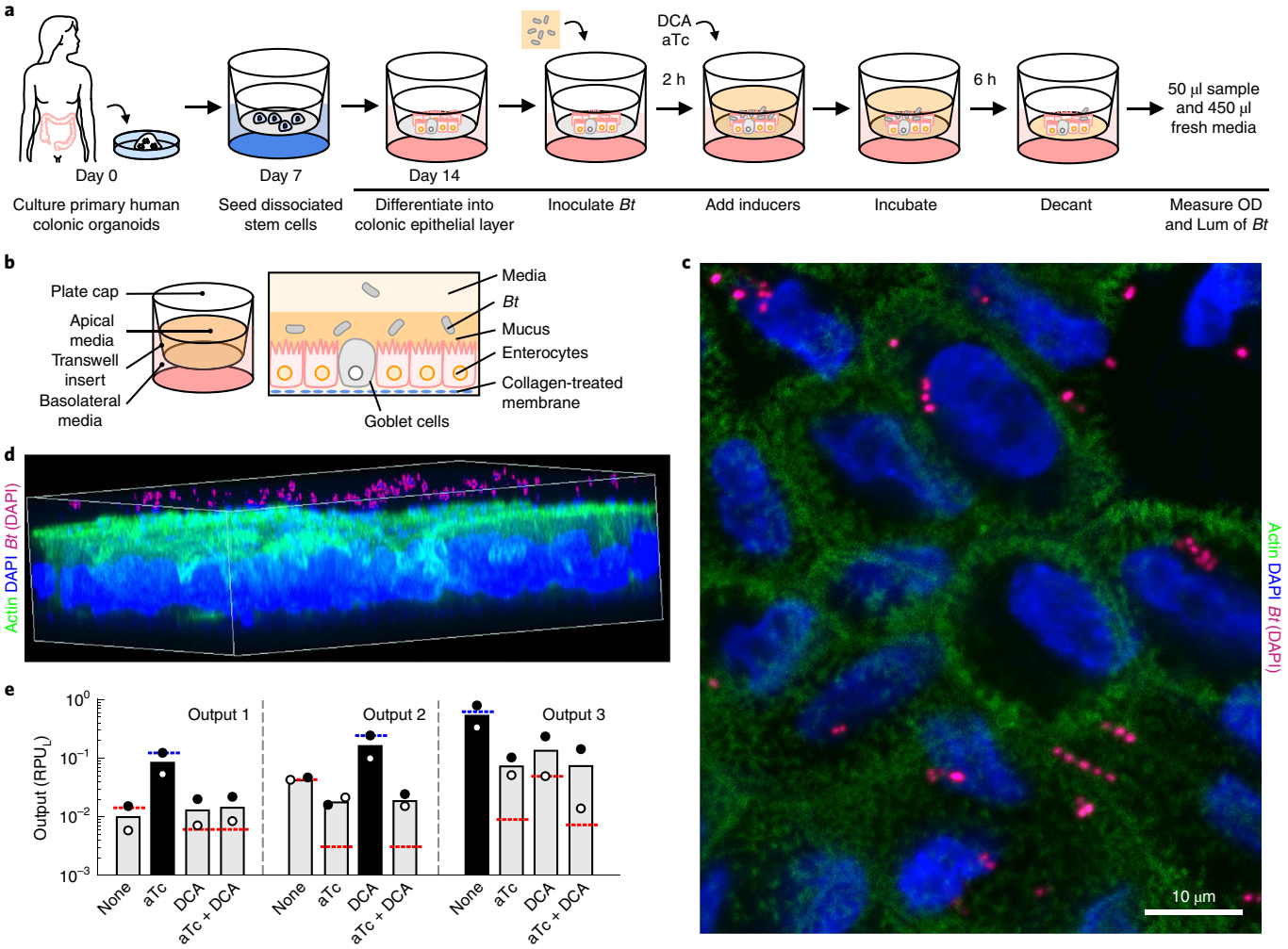

Fig. 4 | Coculture of *B. thetaiotaomicron* with colonic epithelial monolayer. a, Schematic description of the steps to perform the *B. thetaiotaomicron* (MT798, MT799 and MT800; see Supplementary Table 3) and colonic epithelia coculture experiment (Methods). OD, optical density; Lum, luminescence. **b,** An illustration of the human colonic epithelia and *B. thetaiotaomicron* coculture system. **c**, Top view of the monolayer stained with DAPI (blue) and anti-actin (green). *B. thetaiotaomicron* was false colored from blue to pink to highlight their location (see Supplementary Fig. 21 for the original image). **d**, Three-dimensional rendering of the monolayer stained with DAPI and anti-actin (see Supplementary Fig. 22 for the original image). **e**, Outputs of the two-input three-ouput circuit harbored by *B. thetaiotaomicron* cocultured with human colonic epithelia. The predicted values for the three outputs are shown as blue (high) or red (low) lines. Inputs are the presence or absence of 100 ng µl^{-1} aTc and 62.5 µM DCA. The bars show the experimentally measured outputs expected to be low (gray) or high (black). The data represent the average of two replicates collected on different days and white and black circles correspond to each measurement.

(Fig. 3f) across all 12 states representing the 4 combinations of inputs and 3 outputs (Fig. 4e).

We have created a flexible platform to design genetic circuits for *B. thetaiotaomicron*, and have proven its utility by designing a circuit that integrates sensors that respond to a signal of gastrointestinal health and a small molecule pharmaceutical. Although the UCF only has 7 gates, these could be used to build approximately 10^{12} circuits and could be connected to other, user-specified sensors. The circuit output is a reporter gene, but this could be replaced with a gene encoding a therapeutic protein, or gene clusters that build a chemically complex antibiotic or immunomodulator. To date, genetic circuit design automation has been enabled only for a laboratory strain of a model organism (*E. coli*) and a plasmid-based system[6]. Here, we demonstrate that extending circuit design automation to a new species for which there are relatively few genetic tools does not require extensive host characterization. Several circuits were constructed using Cello and, while they were designed to function under specific culture conditions, they were found to function correctly when prototyped under realistic conditions that represent the complexity and uniqueness of the human gut. Our human gastrointestinal model was able to rapidly evaluate the multiple states of the circuit, but this came at the cost of being able to study the circuit response for only 8 h, after which bacterial overgrowth compromised the monolayer. More detailed microphysiological systems could be used to evaluate circuits for up to weeks[67,68]. Furthermore, the complexity of the epithelial layer could be increased to study specific phenomena, such as the response of bacteria residing in crypts, the role of peristalsis and shear stress, molecular transport into the bloodstream, and interactions with the gut–brain axis. The ability to design circuits to specification and then rapidly prototype them under realistic conditions will aid the development of living, responsive human therapeutics.

Online content

Any methods, additional references, Nature Research reporting summaries, source data, extended data, supplementary information,

acknowledgements, peer review information; details of author contributions and competing interests; and statements of data and code availability are available at https://doi.org/10.1038/s41587-020-0468-5.

Received: 18 March 2019; Accepted: 26 February 2020;
Published online: 30 March 2020

References

1. Claesen, J. & Fischbach, M. A. Synthetic microbes as drug delivery systems. *ACS Synth. Biol.* **4**, 358–364 (2015).
2. Mimee, M., Tucker, A. C., Voigt, C. A. & Lu, T. K. Programming a human commensal bacterium, bacteroides thetaiotaomicron, to sense and respond to stimuli in the murine gut microbiota. *Cell Syst.* **1**, 62–71 (2015).
3. Lim, B., Zimmermann, M., Barry, N. A. & Goodman, A. L. Engineered regulatory systems modulate gene expression of human commensals in the gut. *Cell* **169**, 547–558.e515 (2017).
4. Whitaker, W. R., Shepherd, E. S. & Sonnenburg, J. L. Tunable expression tools enable single-cell strain distinction in the gut microbiome. *Cell* **169**, 538–546. e512 (2017).
5. Ruder, W. C., Lu, T. & Collins, J. J. Synthetic biology moving into the clinic. *Science* **333**, 1248–1252 (2011).
6. Nielsen, A. A. et al. Genetic circuit design automation. *Science* **352**, aac7341 (2016).
7. Ozdemir, T., Fedorec, A. J. H., Danino, T. & Barnes, C. P. Synthetic biology and engineered live biotherapeutics: toward increasing system complexity. *Cell Syst.* **7**, 5–16 (2018).
8. Lee, J. W., Chan, C. T. Y., Slomovic, S. & Collins, J. J. Next-generation biocontainment systems for engineered organisms. *Nat. Chem. Biol.* **14**, 530–537 (2018).
9. Piraner, D. I., Abedi, M. H., Moser, B. A., Lee-Gosselin, A. & Shapiro, M. G. Tunable thermal bioswitches for in vivo control of microbial therapeutics. *Nat. Chem. Biol.* **13**, 75–80 (2017).
10. Isabella, V. M. et al. Development of a synthetic live bacterial therapeutic for the human metabolic disease phenylketonuria. *Nat. Biotechnol.* **36**, 857–864 (2018).
11. Riglar, D. T. & Silver, P. A. Engineering bacteria for diagnostic and therapeutic applications. *Nat. Rev. Microbiol.* **16**, 214–225 (2018).
12. Wexler, A. G. & Goodman, A. L. An insider's perspective: Bacteroides as a window into the microbiome. *Nat. Microbiol.* **2**, 17026 (2017).
13. Schwalm, N. D. & Groisman, E. A. Navigating the gut buffet: Control of polysaccharide utilization in bacteroides spp. *Trends Microbiol.* **25**, 1005–1015 (2017).
14. Faith, J. J. et al. The long-term stability of the human gut microbiota. *Science* **341**, 1237439 (2013).
15. Donaldson, G. P., Lee, S. M. & Mazmanian, S. K. Gut biogeography of the bacterial microbiota. *Nat. Rev. Microbiol.* **14**, 20–32 (2015).
16. Jacobson, A. et al. A gut commensal-produced metabolite mediates colonization resistance to salmonella infection. *Cell Host Microbe* **24**, 296–307.e297 (2018).
17. Russell, AlistairB. et al. A type VI secretion-related pathway in bacteroidetes mediates interbacterial antagonism. *Cell Host Microbe* **16**, 227–236 (2014).
18. Ramakrishna, C. *et al. Bacteroides fragilis* polysaccharide A induces IL-10 secreting B and T cells that prevent viral encephalitis. *Nat. Commun.* **10**, 2153 (2019).
19. Wegorzewska, M. M. et al. Diet modulates colonic T cell responses by regulating the expression of a Bacteroides thetaiotaomicron antigen. *Science Immunol.* **4**, eaau9079 (2019).
20. Hamady, Z. Z. R. et al. Xylan-regulated delivery of human keratinocyte growth factor-2 to the inflamed colon by the human anaerobic commensal bacterium *Bacteroides ovatus*. *Gut* **59**, 461–469 (2010).
21. Round, J. L. & Mazmanian, S. K. Inducible Foxp3+ regulatory T-cell development by a commensal bacterium of the intestinal microbiota. *PNAS* **107**, 12204–12209 (2010).
22. Shepherd, E. S., DeLoache, W. C., Pruss, K. M., Whitaker, W. R. & Sonnenburg, J. L. An exclusive metabolic niche enables strain engraftment in the gut microbiota. *Nature* **557**, 434–438 (2018).
23. Qi, LeiS. et al. Repurposing CRISPR as an RNA-guided platform for sequence-specific control of gene expression. *Cell* **152**, 1173–1183 (2013).
24. Daeffler, K. N. M. et al. Engineering bacterial thiosulfate and tetrathionate sensors for detecting gut inflammation. *Mol. Syst. Biol.* **13**, 923 (2017).
25. Riglar, D. T. et al. Engineered bacteria can function in the mammalian gut long-term as live diagnostics of inflammation. *Nat. Biotechnol.* **35**, 653–658 (2017).
26. Archer, E. J., Robinson, A. B. & Süel, G. M. Engineered *E. coli* that detect and respond to gut inflammation through nitric oxide sensing. *ACS Synth. Biol.* **1**, 451–457 (2012).
27. Hwang, I. Y. et al. Engineered probiotic *Escherichia coli* can eliminate and prevent *Pseudomonas aeruginosa* gut infection in animal models. *Nat. Commun.* **8**, 1–11 (2017).
28. Chen, Y. et al. Robust bioengineered 3D functional human intestinal epithelium. *Sci. Rep.* **5**, 1–11 (2015).
29. Leschner, S. et al. Identification of tumor-specific Salmonella Typhimurium promoters and their regulatory logic. *Nucleic Acids Res.* **40**, 2984–2994 (2012).
30. Ozdemir, T. *Design and construction of therapeutic bacterial sensors in* Escherichia coli *Nissle 1917*. PhD thesis, University College London (2018).
31. Kotula, J. W. et al. Programmable bacteria detect and record an environmental signal in the mammalian gut. *PNAS* **111**, 4838–4843 (2014).
32. Kim, S. et al. Quorum sensing can be repurposed to promote information transfer between bacteria in the mammalian gut. *ACS Synth. Biol.* **7**, 2270–2281 (2018).
33. Chen, J. X. *et al.* Development of aspirin-inducible biosensors in *Escherichia coli* and SimCells. *Appl. Environ. Microbiol.* **85**, e02959-18 (2019).
34. Mimee, M., Citorik, R. J. & Lu, T. K. Microbiome therapeutics - Advances and challenges. *Adv. Drug Deliv. Rev.* **105**, 44–54 (2016).
35. Yao, L. *et al.* A selective gut bacterial bile salt hydrolase alters host metabolism. *eLife* **7**, e37182 (2018).
36. Ridlon, J. M., Kang, D. J., Hylemon, P. B. & Bajaj, J. S. Bile acids and the gut microbiome. *Curr. Opin. Gastroenterol.* **30**, 332–338 (2014).
37. Jason M. Ridlon, S. C. H. S. B. D.-J. K., Phillip & Hylemon, B. Consequences of bile salt biotransformations by intestinal bacteria. *Gut Microbes* **7**, 22–39 (2016).
38. Degirolamo, C., Modica, S., Palasciano, G. & Moschetta, A. Bile acids and colon cancer: Solving the puzzle with nuclear receptors. *Trends Mol. Med.* **17**, 564–572 (2011).
39. Kawamata, Y. et al. A G protein-coupled receptor responsive to bile acids. *J. Biol. Chem.* **278**, 9435–9440 (2003).
40. Hofmann, A. F. & Hagey, L. R. Bile acids: chemistry, pathochemistry, biology, pathobiology, and therapeutics. *Cell. Mol. Life Sci.* **65**, 2461–2483 (2008).
41. Hamilton, J. P. et al. Human cecal bile acids: concentration and spectrum. *Am. J. Physiol.* **293**, G256–G263 (2007).
42. Li, T. & Chiang, J. Y. L. Bile acids as metabolic regulators. *Curr. Opin. Gastroenterol.* **31**, 159–165 (2015).
43. Ung, K. A., Gillberg, R., Kilander, A. & Abrahamsson, H. Role of bile acids and bile acid binding agents in patients with collagenous colitis. *Gut* **46**, 170–175 (2000).
44. Bernstein, H., Bernstein, C., Payne, C. M., Dvorakova, K. & Garewal, H. Bile acids as carcinogens in human gastrointestinal cancers. *Mutat. Res.* **589**, 47–65 (2005).
45. Cerda-Maira, F. A., Ringelberg, C. S. & Taylor, R. K. The bile response repressor BreR regulates expression of the vibrio cholerae breAB efflux system operon. *J. Bacteriol.* **190**, 7441–7452 (2008).
46. Gunn, J. S. Mechanisms of bacterial resistance and response to bile. *Microbes Infect.* **2**, 907–913 (2000).
47. Lin, J. et al. Bile salts modulate expression of the CmeABC multidrug efflux pump in campylobacter jejuni. *J. Bacteriol.* **187**, 7417–7424 (2005).
48. Rössger, K., Charpin-El-Hamri, G. & Fussenegger, M. Bile acid-controlled transgene expression in mammalian cells and mice. *Metab. Eng.* **21**, 81–90 (2014).
49. Din, M. O. et al. Synchronized cycles of bacterial lysis for in vivo delivery. *Nature* **536**, 81–85 (2016).
50. Riglar, D. T. et al. Bacterial variability in the mammalian gut captured by a single-cell synthetic oscillator. *Nat. Commun.* **10**, 1–12 (2019).
51. Oberortner, E., Bhatia, S., Lindgren, E. & Densmore, D. A rule-based design specification language for synthetic biology. *J. Emerg. Technol. Comput. Syst.* **11**, 25:21–25:19 (2014).
52. Kelly, J. R. et al. Measuring the activity of BioBrick promoters using an in vivo reference standard. *J. Biol. Eng.* **3**, 4 (2009).
53. Hall, M. P. et al. Engineered luciferase reporter from a deep sea shrimp utilizing a novel imidazopyrazinone substrate. *ACS Chem. Biol.* **7**, 1848–1857 (2012).
54. Cuthbertson, L., Ahn, SangK. & Nodwell, JustinR. Deglycosylation as a mechanism of inducible antibiotic resistance revealed using a global relational tree for one-component regulators. *Chem. Biol.* **20**, 232–240 (2013).
55. Cerda-Maira, F. A., Kovacikova, G., Jude, B. A., Skorupski, K. & Taylor, R. K. Characterization of BreR interaction with the bile response promoters breAB and breR in *Vibrio cholerae*. *J. Bacteriol.* **195**, 307–317 (2013).
56. Stanton, B. C. et al. Genomic mining of prokaryotic repressors for orthogonal logic gates. *Nat. Chem. Biol.* **10**, 99–105 (2014).
57. Nielsen, A. A. K. & Voigt, C. A. Multi-input CRISPR/Cas genetic circuits that interface host regulatory networks. *Mol. Syst. Biol.* **10**, n/a–n/a (2014).
58. Zhang, S. & Voigt, C. A. Engineered dCas9 with reduced toxicity in bacteria: implications for genetic circuit design. *Nucl. Acids Res.* **46**, 11115–11125 (2018).

59. Gander, M. W., Vrana, J. D., Voje, W. E., Carothers, J. M. & Klavins, E. Digital logic circuits in yeast with CRISPR-dCas9 NOR gates. *Nat. Commun.* **8**, 15459 (2017).
60. Liu, Y. et al. Synthesizing AND gate genetic circuits based on CRISPR-Cas9 for identification of bladder cancer cells. *Nat. Commun.* **5**, 5393 (2014).
61. Chen, P.-Y., Qian, Y. & Del Vecchio, D. In *2018 IEEE Conference on Decision and Control (CDC)* 4333–4338 (IEEE, 2018).
62. Chen, Y.-J. et al. Characterization of 582 natural and synthetic terminators and quantification of their design constraints. *Nat. Meth.* **10**, 659–664 (2013).
63. Kozuka, K. et al. Development and characterization of a human and mouse intestinal epithelial cell monolayer platform. *Stem Cell Rep.* **9**, 1976–1990 (2017).
64. Li, H. et al. The outer mucus layer hosts a distinct intestinal microbial niche. *Nat. Commun.* **6**, 1–13 (2015).
65. Fofanova, T. Y. *et al*. A novel human enteroid-anaerobe co-culture system to study microbial-host interaction under physiological hypoxia. Preprint at *bioRxiv* https://doi.org/10.1101/555755 (2019).
66. Srinivasan, B. et al. TEER measurement techniques for in vitro barrier model systems. *J. Lab. Autom.* **20**, 107–126 (2015).
67. Shah, P. et al. A microfluidics-based in vitro model of the gastrointestinal human–microbe interface. *Nat. Commun.* **7**, 11535 (2016).
68. Jalili-Firoozinezhad, S. et al. A complex human gut microbiome cultured in an anaerobic intestine-on-a-chip. *Nat. Biomed. Eng.* **3**, 520–531 (2019).

Methods

Strains, plasmids and media. The *B. thetaiotaomicron VPI-5482 wildtype* (ATCC 29148) strain was used. The backbone vectors, pNBU1-erm and pNBU2-tetQ, were provided by T. Lu (MIT) and M. Fischbach (Stanford University), respectively. All *B. thetaiotaomicron* strains were cultured in TYG broth or brain heart infusion (BHI; BD BBL BHI agar no. 211065) agar supplemented with 10% Horse Blood (Hemostat DHB500). One liter of TYG broth contains 10 g of tryptone peptone (BD Bacto no. 211705), 5 g yeast extract (BD Difco no. 210929), 2 g of glucose (Fisher no. 50-99-7), 100 ml of 1 M KPO_4 (pH 7.2; 11 of the 1 M dibasic (VWR no. 0705-500G) in H_2O and ~430 ml of the 1 M monobasic (Sigma 795488-500G) in H_2O were mixed to achieve pH 7.2), 40 ml of TYG salt solution (0.5 g $MgSO_4 7H_2O$ (USB Corp. no. 18651), 10 g $NaHCO_3$ (Fisher Scientific S233), 2 g of NaCl (Amresco X190) dissolved in 1 l of H_2O), 1 ml of 0.8% $CaCl_2$ (Sigma no. C1016-500G) in H_2O, 1 ml of 0.4 mg ml^{-1} of $FeSO_4$ (Amresco no. 0387-500 G) in H_2O, 4 ml of 0.25 mg ml^{-1} of Resazurin (Sigma no. R7017-1G) in H_2O, 1 ml of histidine-hematin solution (1.2 µg ml^{-1} hematin 12 mg of hematin (Sigma no. H3281-1G) was dissolved in 10 ml of 0.2 M histidine (Sigma no. H7875-25G) in H_2O adjusted to pH 8 and filter sterilized), 0.5 g of L-cysteine (Sigma no. 30089-25 G), and 1 ml of 1 mg ml^{-1} of Menadione (Sigma no. M5625-25G) in 100% ethanol. L-cysteine was resuspended in water (1 ml per 25 mg of L-cysteine) and filter sterilized (0.22 µM filter Pall PN4192) immediately prior to inoculation. Sterile histidine hematin solution, menadione, and L-cysteine were added to the autoclaved media immediately prior to inoculation. Media were pre-reduced (left overnight inside the anaerobic chamber) before inoculation unless otherwise noted. Antibiotics were added as appropriate: erythromycin (25 µg ml^{-1}; Acros Organics no. 114-07-8), tetracycline (2 µg ml^{-1}; Goldbio no. 64-75-5) and gentamicin (200 µg ml−1; Goldbio no. 1405-41-0). Antibiotics for *B. thetaiotaomicron* were used only for post-conjugation selection, and not during growth. The following inducer concentrations were used as appropriate unless otherwise specified: 500 µM IPTG (Goldbio no. 367-93-1), 100 ng ml^{-1} aTc (Acros Organics no. 13803-65-1) and 62.5 µM DCA (Sigma no. D2510-10G). Other bile acids used were CA (Sigma no. C9282-25G), CDCA (Sigma no. C8261-1G), LCA (Sigma no. L6250-10G), TCA (Sigma no. T4009-1G) and GCA (Sigma no. G7132-1G). *E. coli S17-1 λ pir* (from T. Lu) or the EC100D *pir* (VWR no. 75927-934) was used to propagate NBU1- and NBU2-based constructs, and were grown at 37 °C, shaken aerobically in LB (BD Difco no. 244620) broth or LB agar (BD Bacto no. 214010) supplemented with 100 µg ml^{-1} carbenicillin (Goldbio no. 4800-94-6) for post-transformation selection and growth.

Conjugation into *B. thetaiotaomicron* and genome engineering. Constructs based on the pNBU1 and pNBU2 plasmids (Supplementary Fig. 24) were integrated into the *Bacteroides* genome by conjugation using *E. coli S17-1 λ pir*. pNBU1 is based on a *Bacteroides* mobilizable transposon NBU1, containing *intN1* that mediates site-specific recombination of the attN1 site of pNBU1 and the attBT1-1 site in the *B. thetaiotaomicron* genome (located at the 3′ end of tRNA-Leu gene). pNBU1 contains a mutated attN1 where the −2 site has been changed from a G to a C, which has been shown to increase integration frequency. An overnight culture of *E. coli S17-1 λ pir* and *B. thetaiotaomicron* was mixed at a 1:1 ratio in TYG and spot plated on BHI + 10% horse blood agar plates. The matings were incubated aerobically at 37 °C. After >16 h, the cells were scraped and serially streaked onto BHI blood agar plates supplemented with gentamicin and erythromycin for pNBU1 or gentamicin and tetracycline for pNBU2, and incubated anaerobically at 37 °C. Resultant colonies that appeared after 24–48 h were verified for site-specific integration by performing PCR using genome- and vector-specific primers. When both pNBU2 and pNBU1 plasmids were to be integrated into *B. thetaiotaomicron*, pNBU2 was conjugated first followed by pNBU1. All strains constructed for this work are listed in Supplementary Table 3, and their maps illustrated in Supplementary Fig. 24.

Anaerobic growth. All *B. thetaiotaomicron* strains were grown statically in a Forced Air Incubator (Coy Laboratory Model 2000 no. 8543025) at 37 °C inside the anaerobic chamber (Coy Laboratory; Vinyl Anaerobic Chamber Type A Glove Box no. 7000000). Oxygen in the anaerobic chamber was constantly removed by the Palladium Catalyst (Coy Laboratory no. 6501050), which was renewed weekly by incubating in the 90 °C oven for overnight or longer. Nitrogen (Airgas no. NIUHP300) was used to purge air inside the airlock and to maintain a positive pressure in the anaerobic chamber. The oxygen and hydrogen levels in the anaerobic chamber were monitored using the CAM-12 Anaerobic Monitor (Coy Laboratory no. 6250000). The oxygen inside the chamber was maintained at 0 parts per million, unless the inner door of the airlock was opened to move items in and out of the chamber, in which case low levels of oxygen were introduced into the chamber but decreased rapidly. Hydrogen was maintained above 1.5% inside the chamber for proper functioning of the palladium catalyst by adding 5% H_2, 20% CO_2, N_2 gas mix (Airgas Custom Mix, no. X03NI75C2O05502). When moving items in and out of the chamber, the default P1 program (2 cycles of vacuum and purge gas (N_2), followed by 1 cycle of vacuum and gas mix) was used.

Luciferase assay and RPU_L. Overnight *B. thetaiotaomicron* culture in TYGs were diluted 1:100 in fresh TYG and aliquots (180 µl) of *B. thetaiotaomicron* cultures were taken when the OD_{600} was between 0.4 to 0.7 (approximately 6 h). From this culture, 15 µl was mixed with 15 µl of *nanoluc* reaction buffer (Promega Nano-Glo Luciferase System N1120; with substrate added at a 1:50 ratio). The OD_{600} and luminescence were measured using Synergy H1 Hybrid Reader (BioTek no. 8041000). For luminescence reads, 1 s at a gain setting of 100 was used. Both measurements were read on a 96-well flat bottom microtiter plate (Nunc no. 165305). The relative luminescence units (RLU) per colony forming unit (CFU) was calculated by dividing the raw luminescence value by CFU, which was calculated from OD_{600} using a standard curve generated by plotting OD_{600} versus CFU. To convert luciferase activity to RPU_L, an RPU_L standard strain (*B. thetaiotaomicron* strain MT768) was defined (Fig. 1a,b). Luminescence (RLU per CFU) was converted into RPU_L by dividing the luminescence (RLU per CFU) by the luminescence (RLU per CFU) of the RPU_L strain. See the Life Sciences Reporting Summary.

Sensor characterization. DNA encoding CmeR, BreR and the BreR homologs were codon optimized for *B. thetaiotaomicron VPI-5482* using Jcat and synthesized as gBlocks (IDT). Cultures of *B. thetaiotaomicron* containing the sensors were serially streaked onto BHI blood agar plates. A single colony was picked after 24 h and inoculated into 2 ml of TYG (not pre-reduced) in 14 ml Falcon tubes (Fisher no. 14-959-11B) and incubated in the anaerobic chamber at 37 °C statically. Overnight cultures were diluted 1:100 the next day and grown for 6 h in 800 µl of pre-reduced TYG with or without appropriate inducers in PlateOne Deep 96-well 2-ml polypropylene plates (USA Scientific 1896-2000) statically. Aliquots (180 µl) were taken after 6 h and luciferase and OD_{600} were measured (described above). Sensor cross-talk experiments were performed in the same manner. Fold-induction for chemical cross-talk was calculated by dividing the luminescence (RLU/CFU) of the induced culture by that of the uninduced culture. When used as a figure axis label, the term 'Repression (−repressor/+repressor)' refers to the division of the normalized luminescence (RLU/CFU) of a strain lacking a repressor (−repressor) by that measured from a strain containing a repressor (+repressor).

Terminator characterization in *B. thetaiotaomicron*. The luminescence (RLU/CFU) is measured for a strain containing an expression cassette and a strain with a terminator in between the promoter and open reading frame (Supplementary Fig. 12). Glycerol stocks of *B. thetaiotaomicron* containing the terminators were serially streaked onto BHI blood agar plates. A single colony was picked after 24 h and inoculated into 2 ml of TYG (not pre-reduced) in 14-ml Falcon tubes (Fisher no. 14-959-11B) and incubated in the anaerobic chamber statically. Overnight cultures were diluted 1:100 the next day and grown for 6 h in 800 µl of pre-reduced TYG with or without appropriate inducers in PlateOne Deep 96-well 2-ml polypropylene plates (USA Scientific 1896-2000) statically. Aliquots (180 µl) were taken after 6 h and luciferase and OD_{600} were measured (described above).

sgRNA design. A 20-bp random DNA sequence including TANNTTTG was generated using the Random DNA Sequence Generator (http://www.faculty.ucr.edu/~mmaduro/random.htm; GC content probability parameter of 0.5) and was scanned against the *B. thetaiotaomicron VPI-5482* genome with BLASTn to look for off-target sites in the genome that could potentially be affected. No 20-nucleotide sequence had homology to a protospacer-adjacent motif (PAM)-adjacent locus within the genome.

Orthogonality of sgRNAs. All possible combinations of the 7 sgRNA and 7 sgRNA-operator promoters were constructed and conjugated into *B. thetaiotaomicron* strain MT724, resulting in a total of 49 strains (*B. thetaiotaomicron* MT809–MT857). Glycerol stocks of *B. thetaiotaomicron* containing the sgRNA and sgRNA-operator promoter pairs were serially streaked onto BHI blood agar plates. A single colony was picked after 24 h and inoculated into 2 ml of TYG (not pre-reduced) in 14 ml Falcon tubes (Fisher no. 14-959-11B) and incubated in the anaerobic chamber statically. Overnight cultures were diluted 1:100 the next day and grown for 6 h in 800 µl of pre-reduced TYG with or without appropriate inducers in 96 deep well plates statically (USA Scientific 1896-2000). Aliquots (180 µl) were taken after 6 h and luciferase and OD_{600} were measured (described above). Fold repression was calculated by dividing the luminescence of the uninduced culture by the luminescence of the induced *B. thetaiotaomicron* culture.

Gate characterization. The gate measurement plasmids, the RPU_L standard and the bile acid sensor (to convert DCA concentrations to input promoter activity) were all conjugated into *B. thetaiotaomicron* strain MT724. Glycerol stocks of *B. thetaiotaomicron* containing the gates, the RPU_L standard, and the bile acid sensor were serially streaked onto BHI blood agar plates. A single colony was picked after 24 h and inoculated into 2 ml of TYG (not pre-reduced) in 14 ml Falcon tubes (Fisher no. 14-959-11B) and incubated in the anaerobic chamber statically. Overnight cultures were diluted 1:100 the next day and grown for 6 h in 800 µl of pre-reduced TYG in PlateOne Deep 96-well 2-ml polypropylene plates (USA Scientific 1896-2000) statically under a series of DCA concentrations (62.5, 37.5, 22.5, 13.5, 8.1, 4.9, 2.9, 1.7, 1.0, 0.6, 0.4 and 0 µM). Aliquots (180 µl) were

taken after 6 h and luciferase and OD_{600} were measured. The activity of the input promoter against the output promoter was plotted in RPU_L and the Hill function was fit to the data using Prism's nonlinear regression tool and the resulting fit parameters are presented in Supplementary Table 2. Input thresholds 'IL' (input low) and 'IH' (input high), which determine the connectivity of two NOT gates, was initially calculated as the 0.5 times the maximum and 2 times the minimum output, respectively, as described previously[6]. However, for Bth1C1G1T1 UCF, the values were changed to have an IL of 0.001 and IH of 0.2, to increase the number of circuit design solutions that could be found.

Circuit designs using Cello. The Cello software and code are freely available (https://github.com/CIDARLAB/cello). Cello was run locally using the Cello API, and the growth score cutoff was set to 0.75. A UCF file (Bth1C1G1T1.UCF.json) was used (Supplementary File 1). Eugene rules are applied to map gates to linear DNA sequences. To assign the output gate to the 3′ position, rules are included in Eugene such that all of the logic gates are assigned before the output gate (written in Eugene as 'gate_M1 BEFORE gate_nanoluc'). The order of logic gates is random, which is the default option in Eugene. Orientation of each transcription unit is set to be in the same direction and all forward (written in Eugene as 'ALL_FORWARD'). 0.03 RPU_L for no aTc, 6.4 RPU_L for 100 ng ml^{-1} aTc, 0.01 RPU_L for no DCA and 1.5RPU_L for 62.5 µM DCA was used.

Characterizing circuit behavior in a timecourse. Single colonies of *B. thetaiotaomicron* strains harboring RPU_L and the two-input three-output circuit (*B. thetaiotaomicron* MT798, MT799 and MT800 corresponding to reporting output 2, 3 and 1, respectively) were picked and inoculated into TYG (not reduced) without inducers overnight. The next day, 1 ml of the culture was spun down inside the anaerobic chamber (VWR Galaxy minicentrifuge) and the pellets were washed in 1 ml of pre-reduced TYG with aTc twice, and diluted 1:50 into 800 µl of TYG with the same media. OD_{600} and luminescence measurements were taken as described every 2 h for 8 h immediately after inoculating in a new input state. After 8 h, the culture was kept in the anaerobic chamber at 37 °C overnight. The next day, the culture was spun down anaerobically, and again washed twice but with pre-reduced TYG with inducers corresponding to the next input state (DCA only), and diluted 1:50 in TYG with the same media. Again, OD_{600} and luminescence measurements were taken every 2 h for 8 h immediately after the input state transition. This process was repeated for all possible permutations.

Medium for culturing primary colonic epithelial monolayer. Primary colonic epithelial monolayer was maintained by a base medium (DMEM/F12 (Gibco, 12634-010 500 ml) with 5 ml Glutamax –I (Gibco, 35050-061), 5 ml HEPES (Gibco, 15630-080), and 5 ml Pen-Strep (Gibco, 15140-148), an organoid growth medium (Wnt, R-spondin, Noggin (WRN) conditioned medium provided by Boston Children's Hospital (D. Breault), base medium, and 1X B-27 Supplement 50× (Gibco, 17504-001), 1X N-2 Supplement 100× (Gibco, 17502-001), 10 mM nicotinamide (Sigma-Aldrich, N0636), 500 µM *N*-acetyl cysteine (Sigma-Aldrich, A9165), 10 µM Y-27632 dihydrochloride (Biogems, 1293823), 10 µM SB202190 (Biogems, 1523072; Tocris, 1264), 500 nM A 83-01 (Biogems, 9094360), 50 ng ml^{-1} murine EGF (PeproTech, AF-315-09), human [Leu^{15}]-Gastrin I (Sigma-Aldrich, G9145), and 5 nM prostaglandin E2 (Biogems, 3632464)), a seeding medium (seeding medium composition: 65% WRN conditioned medium, 32% base medium, 1X B-27 Supplement 50×, 1X N-2 Supplement 100×, 500 µM *N*-acetyl cysteine, 10 µM SB202190, 2.5 µM thiazovivin, 500 nM A 83-01, 50 ng ml^{-1} murine EGF, human [Leu^{15}]-Gastrin I, 5 nM prostaglandin E2) and a differentiation medium (Differentiation medium composition: 20% R-spondin 1 conditioned medium, 80% base medium (antibiotic free), 1X B-27 Supplement 50×, 1X N-2 Supplement 100×, 500 µM *N*-acetyl cysteine, 500 nM A 83-01, 100 ng ml^{-1} human noggin (PeproTech, 120-10 C), 50 ng ml^{-1} murine EGF, and human [Leu^{15}]-Gastrin I.

Gut epithelial monolayer. The colon monolayer model was derived from primary human colonic stem cell organoids[63]. The cell organoid establishment and maintenance were performed according to previously described methods by the Yilmaz Lab at the Koch Institute and MIT[69]. Normal-appearing regions of endoscopic tissue biopsies collected from the rectosigmoid colon of a de-identified individual (a 30-year-old patient with diverticulitis) at the Massachusetts General Hospital, upon the donor's informed consent. Methods were carried out in accordance with the guidelines of the Koch Institute Institutional Review Board Committee and the Massachusetts Institute of Technology Committee on the Use of Humans as Experimental Subjects. Cell organoids were maintained in Matrigel droplets and passaged every 7 d at a ratio of 1:3. A media change was performed at day 4 after passaging. To prepare the monolayer, organoids were collected into a 15-ml conical tube at day 7. Organoids were pelleted by centrifugation (1,000*g* × 5 min, 4 °C) and then media removal was carried out via aspiration. After that, the Cell Recovery Solution (Corning, 354253; 1 ml per 100 µl Matrigel) was added to disrupt the organoid pellet, and then the organoid suspension was incubated on ice for 45–60 min. The organoid suspension was then pelleted and resuspended with 1 ml pre-warmed $PBS^{-/-}$ (Gibco, 10010-023) containing 2.5 mg ml^{-1} Trypsin (Sigma, T4549) and 0.45 mM EDTA (Ambion, AM9260G). The resuspended organoids were placed in a 37 °C water bath for 5 min and then manually dissociated into single cells using a 1,000-µl pipette with a bent tip. Cells were counted with TrypanBlue and automated cell counter (Invitrogen). Cells were diluted to a density of 600,000 cells per ml in seeding media and 500 µl was added into the apical side of each 12-well coated transwell (surface area: 1.12 cm^2) and 1.5 ml cell-free seeding medium was added to the basolateral side. Prior to seeding, transwells were coated with rat tail collagen I (Gibco, A10483-01, 50 µg ml^{-1} in PBS) for 1–2 h in the incubator, then was washed with PBS immediately before adding the cells.

Coculture of primary colonic epithelial monolayer and *B. thetaiotaomicron*. Differentiated monolayers were used for the coculture with *B. thetaiotaomicron*. At day 3 after seeding, the monolayers were differentiated by exchanging antibiotic-free base medium on the apical side and differentiation medium on the basolateral side. The differentiated monolayers (4–5 d after cell differentiation) were used for epithelia–*B. thetaiotaomicron* coculture. *B. thetaiotaomicron* cells were grown as described above except TYG medium or BHI agar plates were replaced by YCFA medium (AS-680, Anaerobe Systems) or YCFA agar plates (AS-675, Anaerobe Systems). TYG media was not used because preliminary experiments suggested TYG media alone compromises the monolayer. *B. thetaiotaomicron* cells were resuspended in 500 µl of YCFA containing no inducers and then added into the apical side of the monolayer. Prior to adding *B. thetaiotaomicron* cells, the apical media was aspirated. The monolayers were then immediately transferred into the incubator (5% CO2, 37 °C). After incubating for 2 h, inducers were added to the media and incubated for another 6 h. After 6 h, 450 µl of the top apical medium was removed, and 50 µl of the medium containing the cells settling on the surface of the epithelial cells were diluted and mixed with 450 µl of fresh YCFA. OD_{600} and luminescence were measured as described above. After collecting *B. thetaiotaomicron*, TEER was measured by adding 500 µl PBS and placing the transwell into the EndOhm chamber connected to the EVOM2 Epithelial Voltohmmeter. See the Life Sciences Reporting Summary.

Immunofluorescence staining and imaging. The monolayer was fixed with 4% formaldehyde for 10 min. To block the non-specific binding, the fixed cells were then cultured with BlockAid blocking solution (Thermo Fisher B10710) for 1 h with gentle shaking (50 r.p.m.). Afterwards, cells were stained with conjugated phalloidin (ab176753) and DAPI diluted in blockade solution and incubated at 4 °C overnight with aluminum foil cover. Cells were washed twice the next day with PBS, 5 min each. Then the membrane with monolayer was cut out from the transwell insert, mounted on a glass and covered with thin circular glass slip after adding a drop of antifade solution. Imaging was performed using a Zeiss LSM 880 confocal microscope. The three-dimensional image was rendered using the software Zen 2.3 SP1 FP3, version 14.0.20.201 (Zeiss). Brightfield images were taken with EVOS cell imaging system. For Fig. 4c,d, the bacteria in the image were specifically false colored from the DAPI blue color to pink using GIMP-2.10 to highlight the bacteria relative to the mammalian cells. Brightness and contrast were also increased.

Reporting Summary. Further information on research design is available in the Nature Research Reporting Summary linked to this article.

Data availability

Genetic parts and the UCF file Bth1C1G1T1 are available as Supplementary Information. The DNA sequences for the following plasmids are deposited into GenBank: pMT405 (MN991273); pMT406 (MN991274); pMT423 (MN991275); pMT444 (MN991276); pMT445 (MN991277); pMT447 (MN991278); pMT448 (MN991279); pMT449 (MN991280); pMT450 (MN991281); pMT451 (MN991282); pMT455 (MN991283); pMT462 (MN991284); pMT468 (MN991285); pMT469 (MN991286); pMT470 (MN991287); pMT492 (MN991288); pMT493 (MN991289); pMT494 (MN991290).

Code availability

The Cello software and codes are freely available (https://github.com/CIDARLAB/cello).

References

69. Roper, J. et al. In vivo genome editing and organoid transplantation models of colorectal cancer and metastasis. *Nat. Biotechnol.* **35**, 569–576 (2017).

Acknowledgements

We thank M. Mimee (MIT) and T. Lu (MIT) for providing us with the NBU1-based *Bacteroides* shuttle vector pNBU1-Erm. We thank M. Fischbach (Stanford University) for providing us with the NBU2-based *Bacteroides* shuttle vector pNBU2-tetQ. Primary human colonic epithelial cells were obtained by generous contributions from the laboratory of O. Yilmaz (MIT). We thank K. Schneider (MIT) and C. Wright (MIT) for technical assistance. This work was supported by the National Institute of Health P50 grant (P50-GM098792), Office of Naval Research Multidisciplinary University

Research Initiatives Program (N00014-13-1-0074), Defense Agency Research Projects Agency Synergistic Discovery and Design (SD2; FA8750-17-C-0229), National Science Foundation Semiconductor Synthetic Biology for Information Processing and Storage Technologies (SemiSynBio; CCF-1807575) program and National Institutes of Health (NIH R01EB021908).

Author contributions

M.T. and C.A.V. conceived the project and designed experiments. J.Z., Y.H. and L.G. built the in vitro gut model system. M.T., A.T., J.Z. and Y.H. performed the experiments. S.Z. performed the computational work. M.T., S.Z., J.Z. and C.A.V. wrote the manuscript.

Competing interests

C.A.V. and M.T. have filed a provisional patent based on this work. All other authors have no competing interests.

Additional information

Supplementary information is available for this paper at https://doi.org/10.1038/s41587-020-0468-5.

Correspondence and requests for materials should be addressed to C.A.V.

Reprints and permissions information is available at www.nature.com/reprints.

nature research

Corresponding author(s): *Double-blind peer review submissions: write DBPR and your manuscript number here instead of author names.*

Last updated by author(s): *YYYY-MM-DD*

Reporting Summary

Nature Research wishes to improve the reproducibility of the work that we publish. This form provides structure for consistency and transparency in reporting. For further information on Nature Research policies, see Authors & Referees and the Editorial Policy Checklist.

Statistics

For all statistical analyses, confirm that the following items are present in the figure legend, table legend, main text, or Methods section.

n/a	Confirmed
☐	☒ The exact sample size (*n*) for each experimental group/condition, given as a discrete number and unit of measurement
☐	☒ A statement on whether measurements were taken from distinct samples or whether the same sample was measured repeatedly
☒	☐ The statistical test(s) used AND whether they are one- or two-sided *Only common tests should be described solely by name; describe more complex techniques in the Methods section.*
☒	☐ A description of all covariates tested
☒	☐ A description of any assumptions or corrections, such as tests of normality and adjustment for multiple comparisons
☐	☒ A full description of the statistical parameters including central tendency (e.g. means) or other basic estimates (e.g. regression coefficient) AND variation (e.g. standard deviation) or associated estimates of uncertainty (e.g. confidence intervals)
☒	☐ For null hypothesis testing, the test statistic (e.g. *F*, *t*, *r*) with confidence intervals, effect sizes, degrees of freedom and *P* value noted *Give P values as exact values whenever suitable.*
☒	☐ For Bayesian analysis, information on the choice of priors and Markov chain Monte Carlo settings
☒	☐ For hierarchical and complex designs, identification of the appropriate level for tests and full reporting of outcomes
☐	☒ Estimates of effect sizes (e.g. Cohen's *d*, Pearson's *r*), indicating how they were calculated

Our web collection on statistics for biologists contains articles on many of the points above.

Software and code

Policy information about availability of computer code

Data collection	Biotek Gens was used to collect luminescence and OD600 data.
Data analysis	The Cello software was used for designing the genetic circuits. Microsoft Excel 16.16.7 and Prism 7.0a was used to analyze data, compute statistics, and generate graphs. 3D image was rendered using Zeiss Zen 2.3 SP1 FP3, version 14.0.20.201.

For manuscripts utilizing custom algorithms or software that are central to the research but not yet described in published literature, software must be made available to editors/reviewers. We strongly encourage code deposition in a community repository (e.g. GitHub). See the Nature Research guidelines for submitting code & software for further information.

Data

Policy information about availability of data

All manuscripts must include a data availability statement. This statement should provide the following information, where applicable:

- Accession codes, unique identifiers, or web links for publicly available datasets
- A list of figures that have associated raw data
- A description of any restrictions on data availability

Genetic parts and the UCF file BthlClGlTl are available as Supplementary Information. Selected plasmids and strains will be available on Addgene (https://www.addgene.org/Christopher_Voigt/). The DNA sequences for the following plasmids are deposited into Genbank: pMT405 (MN991273); pMT406 (MN991274); pMT423 (MN991275); pMT444 (MN991276); pMT445 (MN991277); pMT447 (MN991278); pMT448 (MN991279); pMT449 (MN991280); pMT450 (MN991281); pMT451 (MN991282); pMT455 (MN991283); pMT462 (MN991284); pMT468 (MN991285); pMT469 (MN991286); pMT470 (MN991287); pMT492 (MN991288); pMT493 (MN991289); pMT494 (MN991290). The data that support the findings of this study are available from the corresponding author upon reasonable request.

Field-specific reporting

Please select the one below that is the best fit for your research. If you are not sure, read the appropriate sections before making your selection.

☒ Life sciences ☐ Behavioural & social sciences ☐ Ecological, evolutionary & environmental sciences

For a reference copy of the document with all sections, see nature.com/documents/nr-reporting-summary-flat.pdf

Life sciences study design

All studies must disclose on these points even when the disclosure is negative.

Sample size	Statistical methods were not used to predetermine sample size. All main experiments were performed in triplicates on different days.
Data exclusions	No data were excluded from the manuscript.
Replication	Experiments were replicated at least three times on different days using the reported methods All results were reliably replicated.
Randomization	Randomization was not performed in our study as it was not relevant. We compared the reporter levels of the specified engineered strains in a given experiment simultaneously and in the same manner.
Blinding	Blinding was not done because it was not conducive to this work.

Reporting for specific materials, systems and methods

We require information from authors about some types of materials, experimental systems and methods used in many studies. Here, indicate whether each material, system or method listed is relevant to your study. If you are not sure if a list item applies to your research, read the appropriate section before selecting a response.

Materials & experimental systems

n/a	Involved in the study
☒	☐ Antibodies
☒	☐ Eukaryotic cell lines
☒	☐ Palaeontology
☒	☐ Animals and other organisms
☒	☐ Human research participants
☒	☐ Clinical data

Methods

n/a	Involved in the study
☒	☐ ChIP-seq
☒	☐ Flow cytometry
☒	☐ MRI-based neuroimaging